IEEE Access
Multidisciplinary ⋮ Rapid Review ⋮ Open Access Journal

Received November 21, 2021, accepted December 4, 2021, date of publication December 14, 2021,
date of current version December 22, 2021.

Digital Object Identifier 10.1109/ACCESS.2021.3135574

LVRT Control Strategy for Asymmetric Faults of DFIG Based on Improved MPCC Method

CAN DING, YUNWEN CHEN, AND TAIPING NIE
College of Electrical Engineering and New Energy, China Three Gorges University, Yichang 443002, China
Corresponding author: Can Ding (dingcan@ctgu.edu.cn)

ABSTRACT In the case of asymmetric fault, the modern new power grid requires that the doubly-fed induction generator (DFIG) still has good low voltage ride-through (LVRT) capabilities. To solve this problem, a low voltage ride-through control strategy based on an improved model predictive current control method in the two-phase stationary coordinate system is proposed in this paper. Firstly, the transient characteristics of DFIG are analyzed, and an improved flux extraction method is proposed. The traditional flux linkage measurement link is simplified by the method and the one-beat delay problem of model predictive control is solved by controlling the step length. Then, the induced voltage and flux attenuation are introduced into the model predictive control method. It can effectively eliminate the double-frequency oscillation component in the DC bus voltage and electromagnetic torque. Therefore, the grid-connected power quality is improved. Finally, an example shows that the control strategy has a good effect on the realization of LVRT under asymmetric faults. The two control goals of self-preservation and support of a double-fed induction generator during low voltage ride-through can be achieved.

INDEX TERMS Doubly-fed induction generator, low voltage ride-through, predictive current control, flux measurement, two-phase stationary coordinate system.

I. INTRODUCTION

Wind energy has the characteristics of randomness and volatility. In the process of grid-connected power generation, it presents shortcomings such as strong output power fluctuations and large impacts on the grid, which will affect the normal operation of the grid [1]. Therefore, modern power grids place high requirements on the grid-connected operation of wind turbines, requiring wind turbines to have high reactive power control capabilities [2]–[4], [6], [7] and low voltage ride-through capabilities during faults [5], [8]–[10]. The technical difficulty of a DFIG operating in LVRT is to achieve the following two control goals at the same time, namely self-protection and support. Self-protection mainly suppresses stator and rotor overcurrent, rotor overvoltage, and DC bus overvoltage, and protects the safety of the rotor side converter (RSC) and DC bus capacitor. The support is to continuously and stably provide reactive power to assist the grid voltage recovery and reduce the possibility of grid voltage collapse [11].

At present, scholars usually improve the control strategy of the excitation converter to achieve the purpose of protecting wind turbines. Its advantage is to make full use of the capacity of the DFIG to achieve LVRT. However, when the degree of failure exceeds the capacity of the converter, hardware equipment will be added as an auxiliary control. A method for calculating the reference current of the grid side converter (GSC) using the PR controller in the $\alpha\beta$ coordinate system was proposed in [2]. It is used for GSC to compensate for reactive power, but it only controls the grid-connected power quality and output power. A control strategy for active and reactive power during the fault process was proposed in [3]. When the rotor current exceeds the threshold, the crowbar will be used for auxiliary control. The series resonance fault current limiter (SRFCL) framework designed in [4] effectively reduces the reactive power required for wind energy absorption from the grid during a fault. A new topology to enhance the capability of fixed-speed induction generator-based wind turbines (FSIG-WT) during fault ride-through (FRT) was proposed in [6]. The auxiliary controller proposed in [7] does not need to change the original structure of the voltage controller. It controls the exchange of actual reactive power according to the grid standard. A voltage compensation control strategy based on the nine-switch converter was proposed in [5] to improve the LVRT capability of the DFIG. The basic requirements of active power control and reactive

The associate editor coordinating the review of this manuscript and approving it for publication was Ramani Kannan.

power compensation were emphatically studied [8]. These requirements have a special impact on the operation of wind energy. An advanced PSO algorithm and K-means clustering algorithm to achieve LVRT were used in [9]. It analyzes the vital role played by the Crowbar circuit during fault and grid restoration. The crowbar makes the output power smoother. A grid adaptability test method for wind turbines was developed in [10]. It avoids the negative impact of unbalanced voltage on the induction generator and rotor converter. The above control strategy has been improved to some extent during LVRT, such as improving the quality of grid-connected power or effectively suppressing the phenomenon of overvoltage. However, they have not achieved reactive power control at the same time while suppressing rotor overvoltage and other phenomena. In addition, the control strategy in [3], [4], [6] is not only improved but also the investment of hardware equipment is increased or the topology is changed. This greatly increased the cost of hardware. The essence of fault control is to suppress the DC component of the flux linkage caused by the fault, which is not analyzed in the above papers. Some new control technologies such as internal model [12], hysteresis [13], [14], and sliding mode [15] control have been proposed one after another. Compared with traditional PI controllers, these control techniques have great advantages in suppressing rotor overcurrent, but they cannot accelerate stator transient flux decay. The concept of optimal demagnetization was proposed in [16]. By selecting the appropriate demagnetization coefficient, the current peak value of the generator-side converter during the low voltage ride-through is minimized. To support the restoration of the grid voltage, scholars superimposed the de-excitation current command with the normal rotor current command [17]. It completed de-excitation control and reactive power support while controlling the rotor converter, but the scheme required a larger current capacity of the GSC. A de-excitation control method based on grid voltage-oriented vector control is introduced in [18]. This method can speed up the attenuation speed of the stator flux linkage. But in this paper, only the simulation study on the control of the three-phase symmetrical drop of the grid voltage was carried out, and the study of the asymmetric drop condition was not carried out.

Model predictive control (MPC) is an optimization algorithm [19]. Its principle is to predict the future state values and output values according to the built system model, and then carry out the rolling optimization of the control quantity according to the evaluation function, and finally select the optimal control algorithm. Scholars introduced a model predictive control method applied to the field of power electronics [20]. This paper described in detail the application of finite control set-model predictive control (FCS-MPC) to power converters. Some scholars have designed a predictive control strategy based on the maximum wind energy tracking model of the DFIG. This strategy kept the output power of the wind turbine stable when the wind speed changes, but did not apply the MPC to the excitation converter of the wind turbine. Some scholars combined MPC with demagnetization control, but the flux linkage measurement link is complicated, which affected the demagnetization effect [21], [22]. Other scholars proposed improved demagnetization control [23]. The control system will dynamically adjust the demagnetization proportional coefficient according to the depth of the grid voltage drop, but this control method is only suitable for symmetrical faults.

An improved model predictive current control (MPCC) strategy based on a two-phase stationery ($\alpha\beta$) coordinate system under asymmetrical power grid faults is proposed in this paper. The complex flux measurement problems of DFIG during LVRT and the problems of delay and large computation in MPC control process were solved by this strategy. First, a reference model was established based on the structure of the DFIG to analyze its dynamic process in the case of asymmetrical faults in the power grid. Then the predictive model based on dynamic analysis was built, and the control step length was set to the most suitable step length that can offset the delay problem. And a new method of flux linkage measurement was proposed in this paper. This method controlled the rotor flux linkage to track the stator flux linkage decay, to achieve the purpose of suppressing the rotor overcurrent and suppressing the flux linkage fluctuation. The fault ride-through control strategy was designed as described above. Finally, it was verified on the MATLAB/Simulink simulation platform that the control strategy can guarantee the feasibility of support while protecting itself.

The control strategy proposed in this paper is different from the traditional controller which only analyzes aspects such as reactive power support or overvoltage. The attenuation of the flux linkage is added to the fault analysis and controlled. And it combines the MPCC with traditional control. This enables the control under the fault to be scrolled and optimized to obtain a better control process. At the same time, the delay problem of the model predictive control is also suppressed to a certain extent. This paper conducts simulation research on the transient model of asymmetric faults. The simulation results show that the rotor overvoltage and overcurrent phenomenon in the case of asymmetric faults can be suppressed to a certain extent by the control strategy. The DC bus voltage fluctuation and the double frequency oscillation in the electromagnetic torque are also effectively suppressed, thereby improving the grid-side power quality under the fault.

II. ANALYSIS OF TRANSIENT CHARACTERISTICS OF DFIG IN POWER GRID FAILURE

A. MATHEMATICAL MODEL OF DFIG IN $\alpha\beta$ COORDINATE SYSTEM

To obtain a complete DFIG model, the parameters are equivalent to the stator coordinate system, and the motor convention is adopted. The mathematical model of DFIG in the three-phase stationary coordinate system can be written as

$$\begin{aligned} u_s &= R_s i_s + \frac{d\varphi_s}{dt} \\ u_r &= R_r i_r + \frac{d\varphi_r}{dt} - j\omega_r \varphi_r \end{aligned} \tag{1}$$

$$\begin{aligned}\varphi_s &= L_s i_s + L_m i_r \\ \varphi_r &= L_r i_r + L_m i_s\end{aligned} \tag{2}$$

Among them, u_s and u_r are the stator and rotor side voltages, i_s and i_r are the stator and rotor side currents, R_s and R_r are the stator and rotor resistances, φ_s and φ_r are stator and rotor flux linkages respectively, L_s and L_r are the stator and rotor inductances respectively, L_m is the stator and rotor mutual inductances, and ω_r is the rotor speed.

According to the mathematical model of the DFIG in the three-phase stationary coordinate system, it can be seen that the model is not only a time-varying or coupled, but also a nonlinear equation. These characteristics are not conducive to the design of the controller, so coordinate transformation is needed to simplify the model. The model is transformed from the three-phase stationary coordinate system to the two-phase stationary coordinate system, and a mathematical model of vector control is built for its stable operation. The subsequent optimization control algorithms in this paper are all carried out in the $\alpha\beta$ coordinate system. In the two-phase stationary coordinate system, the control strategy can save Park coordinate transformation and reduce the introduction of parameter θ_r in the calculation. In addition, the conventional stator flux orientation method is affected by the cross-coupling term of the positive sequence component in the counterclockwise rotating synchronous coordinate system. When the load is unbalanced, it appears as harmonics in the d-q coordinate system. Therefore, it is necessary to control the current in the d-q coordinate system. The feedforward decoupling of the cross-coupling is performed, and the controller design at this time becomes complicated. Rewriting equation (1), the mathematical model of the stator side and rotor side of the DFIG in the $\alpha\beta$ reference frame is expressed as follows:

$$\begin{aligned}u_{s\alpha\beta} &= R_s i_{s\alpha\beta} + \frac{d\varphi_{s\alpha\beta}}{dt} \\ u_{r\alpha\beta} &= R_r i_{r\alpha\beta} + \frac{d\varphi_{r\alpha\beta}}{dt} - j\omega_r \varphi_{r\alpha\beta}\end{aligned} \tag{3}$$

Rewritten equation (2), the stator and rotor flux linkages in the $\alpha\beta$ reference system is expressed as follows:

$$\begin{aligned}\varphi_{s\alpha\beta} &= L_s i_{s\alpha\beta} + L_m i_{r\alpha\beta} \\ \varphi_{r\alpha\beta} &= L_r i_{r\alpha\beta} + L_m i_{s\alpha\beta}\end{aligned} \tag{4}$$

According to the state space equations of stator flux linkage and rotor flux linkage, it can be deduced that the following relationship exists:

$$\varphi_{r\alpha\beta} = \frac{L_r}{L_m}\varphi_{s\alpha\beta} + \sigma L_m i_{s\alpha\beta} \tag{5}$$

where σ is the leakage inductance coefficient, $\sigma = \frac{1-L_m^2}{L_s L_m}$. The relationship of the rotor flux linkages is $\varphi_{r\alpha\beta} = \varphi_{r\alpha} + j\varphi_{r\beta}$.

In the same way, the relationship between the rotor voltage and the stator flux linkage is obtained:

$$u_r = \frac{L_m}{L_s}\frac{d\varphi_s}{dt} + (\sigma L_r + R_r)\, i_r \tag{6}$$

In the $\alpha\beta$ coordinate system, the active and reactive power output from the stator side of the DFIG are respectively:

$$P_s + jQ_s = -\frac{3}{2}u_{s\alpha\beta} \times \hat{i}_{s\alpha\beta} \tag{7}$$

where

$$\begin{aligned}P_s &= -\frac{3}{2}\left(u_{s\alpha} i_{s\alpha} + u_{s\beta} i_{s\beta}\right) \\ Q_s &= -\frac{3}{2}\left(u_{s\beta} i_{s\alpha} - u_{s\alpha} i_{s\beta}\right)\end{aligned}$$

According to the above, the state space equations of the DFIG after grid connection are obtained, and these equations can be used as the model basis of the improved MPCC strategy.

The DFIG often uses steady-state stator flux orientation vector control during LVRT. However, this control strategy ignores the transient process of the stator flux linkage of the DFIG, and the stator flux linkage cannot be accurately oriented when the fault occurs, so it is not suitable for the operation of the DFIG when the fault occurs.

B. DYNAMIC ANALYSIS OF ASYMMETRICAL POWER GRID FAULTS

Compared with the three-phase symmetrical drop, the stator flux contains a negative sequence component during an asymmetrical drop of the power grid. The existence of the negative-sequence component of the flux linkage makes the negative-sequence component of the grid voltage relative to the rotor have a greater slip rate, which will lead to more serious rotor overvoltage and overcurrent. Therefore, the control of LVRT under asymmetric faults should be paid more attention to.

Equation (3) is also valid under unbalanced faults, and it can be written in the following equation:

$$\begin{aligned}u_{r\alpha} &= R_r i_{r\alpha} + \frac{d\varphi_{r\alpha}}{dt} + \omega_r \varphi_{r\beta} \\ u_{r\beta} &= R_r i_{r\beta} + \frac{d\varphi_{r\beta}}{dt} - \omega_r \varphi_{r\alpha}\end{aligned} \tag{8}$$

Combining equation (3) and equation (5), after eliminating the rotor flux, equation (8) can be rewritten as:

$$\begin{aligned}u_{r\alpha} &= R_r i_{r\alpha} + \left(L_r - \frac{L_m^2}{L_s}\right)\left(\frac{di_{r\alpha}}{dt} + \omega_r i_{r\beta}\right) \\ &\quad + \underbrace{\frac{L_m}{L_s}\left(\frac{d\varphi_{s\alpha}}{dt} + \omega_r \varphi_{s\beta}\right)}_{e_{r\alpha}} \\ u_{r\beta} &= R_r i_{r\beta} + \left(L_r - \frac{L_m^2}{L_s}\right)\left(\frac{di_{r\beta}}{dt} - \omega_r i_{r\alpha}\right) \\ &\quad + \underbrace{\frac{L_m}{L_s}\left(\frac{d\varphi_{s\beta}}{dt} - \omega_r \varphi_{s\alpha}\right)}_{e_{r\beta}}\end{aligned} \tag{9}$$

The rotor voltage is composed of two parts, which can be seen from equation (9). They are the rotor back electromotive force related to the stator flux and the rotor loop voltage drop

determined by the rotor current and rotor winding parameters. That is to say, the vector of the rotor voltage is determined by both the stator flux linkage and the rotor current. This is consistent with the influence factor of equation (6) on the rotor voltage.

When an asymmetric fault occurs in the power grid, the stator flux linkage can be divided into three flux linkages. Two of them are determined by the stator voltage, which are the positive sequence flux φ_{s1} rotating in the positive sequence of ω_s and the negative sequence flux φ_{s2} rotating in the negative sequence of $-\omega_s$. The remaining part is free flux φ_{sf}. The slip rate of the stator transient DC flux linkage and negative sequence AC flux linkage is much greater than the normal stator flux linkage. A large transient back electromotive force will be induced in the rotor winding during flux rotation. This back electromotive force eventually leads to overcurrent of the rotor and relatively large electromagnetic torque pulsation is caused at the same time. The traditional PI controller only controls the positive sequence component, and the simultaneous control of the positive and negative sequence components cannot be realized. Therefore, the control method of the sequence component is improved in this paper. The total stator flux is derived from the mathematical model of DFIG in the three-phase static coordinate system [24], which is equation (1). The stator flux is changed to an integral term:

$$\varphi_s = \int (u_s - R_s i_s) dt \tag{10}$$

Since the free component of the flux linkage is a DC component with a relatively slow-changing speed, it can be obtained by filtering with a low-pass filter. At this time, the combined value of the free component and the negative sequence component of the flux linkage can be obtained, as shown in the following equation:

$$\varphi_s - \frac{1}{j\omega_s}\frac{d\varphi_s}{dt} = 2\varphi_{s2} + \varphi_{sf} \tag{11}$$

Rewrite the above equation as:

$$\varphi_s = \omega_s \int \sqrt{\left(2\varphi_{s2} + \varphi_{sf}\right)^2 - \varphi_s^2} dt \tag{12}$$

Equation (12) is discretized, and the sampling period is T_s, where $T_s = 50\mu s$. Then the trapezoidal equation is introduced. The results will be used as the kth flux linkage value in the subsequent predictive control process, and the following flux linkage measurement method can be obtained:

$$\begin{aligned} \alpha_{(k)} &= \sqrt{\left(\frac{2\varphi_{s(k)}}{\omega_s T_s}\right)^2 + \varphi_{s(k)}^2} \\ \varphi_{s2(k)} &= \frac{1}{2}\left[\alpha_{(k)} - \varphi_{sf(k)}\right] \\ \varphi_{s(k)} &= \varphi_{s1(k)} + \varphi_{s2(k)} + \varphi_{sf(k)} \end{aligned} \tag{13}$$

The flux measurement process is shown in Figure 1.

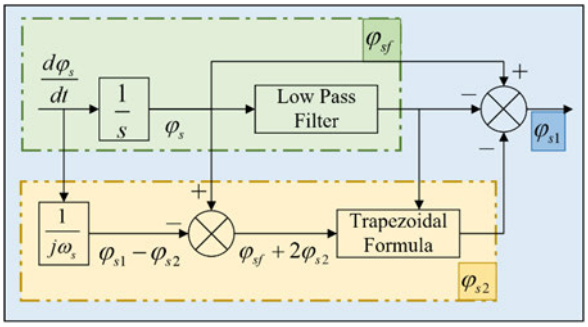

FIGURE 1. Flux link measurement link structure.

III. IMPROVED MODEL PREDICTIVE CURRENT CONTROL

The principle of predictive control is divided into three basic steps. First, a predictive model is established, then the future dynamics of the system are predicted, and finally, the results of constraints after optimization are applied to the system.

A. BUILD A PREDICTIVE MODEL

According to the principle of model predictive control, the time interval P in the forecast time domain should not be less than the time interval M in the control time domain, that is, $P \geq M$. Considering the delay problem of model predictive control, the time interval of the control time domain is shortened in this paper. It is mentioned that the model predictive current control has the characteristic that it is almost impossible to obtain the control current of the next 3 cycles in the kth cycle [25]. No matter if the sampling time of the converter is shortened to 1/2Ts or 1/4Ts, its control current is consistent with the kth current. Moreover, the MPC can only make a trade-off in terms of stability and rapidity, which means that the two cannot be perfectly compatible [26]. If the sampling frequency is too high, high requirements will be imposed on the control chip, and the control system will have a large error at this time [27]. To make the excitation converter have as fast a response speed as possible, and the one-beat delay problem in the timing control should be considered [28], the sampling time of the excitation converter to $1/2T_s$ is shortened in this paper. At this time, the prediction time-domain P is equal to $2M$. It applies the optimal combination of switching functions at time $t(k+1)$ determined at time $t(k)$ to time $t(k+2)$, thereby an ideal combination of switching functions is obtained. The derivation of the prediction equation is shown in Figure 2. Among them: $x(k)$ is the sampling time; $i(k)$ is the sampling current corresponding to the sampling time; $i(4)$ is the current sampling value; $i(m)$ is the predicted current value; $x(k) - x(k-1) = T_s/2$; $x(m) - x(4) = T_s/2$. The principle of action in Figure 2 is that $i(3)$ is sampled at $x(3)$. It is predicted that the control value at time $x(4)$ will be applied at time $x(m)$. The obtained control value $i(4)$ will be directly compared by the value function to obtain the final control signal. In the event of a fault, the current value fluctuates in a large range. The repeated iterations of model prediction make the value at each moment be effectively processed. The predicted value

is essentially the result of processing based on the value obtained at the current time $x(3)$. And the predicted value belongs to the future value, so it will not affect the prediction model at the current moment.

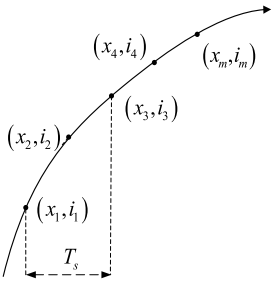

FIGURE 2. Schematic diagram of prediction formula derivation.

To realize improved MPCC of LVRT, the voltage and current are firstly sampled discretely to obtain:

$$\frac{d}{dt}\begin{bmatrix} u \\ i \end{bmatrix} = \frac{1}{T_s}\begin{bmatrix} u(k) - u(k-1) \\ i(k) - i(k-1) \end{bmatrix} \tag{14}$$

Compared with other controllers, the positive and negative sequence of voltage and current does not need to be separated from the improved MPCC strategy proposed in this paper. This avoids the problem that the separation of positive and negative sequence cannot be accurately controlled when the voltage drops. The state-space model of a linear discrete-time system is written as follows:

$$\begin{aligned} x(k+1) &= Ax(k) + B_u u(k) + B_d d(k) \\ y_c(k+1) &= C_c x(k) \end{aligned} \tag{15}$$

where $x(k)$ is the state variable, $u(k)$ is the input control variable, $y_c(k)$ is the controlled output variable, and $d(k)$ is the measurable external disturbance variable. The current $i_{r\alpha}(k)$, $i_{r\beta}(k)$ and other information are used as the state variable matrix $x(k)$. The mathematical model of the doubly-fed machine is used as the input control variable $u(k)$. Based on the above parameters, the current values $i_{r\alpha}(k+1)$ and $i_{r\beta}(k+1)$ at the next moment are predicted, and the predicted results will be used as the controlled output variable $y_c(k)$. First of all, it is assumed that all state variables of the system can be measured in this paper, and the above equations are rewritten as an incremental model:

$$\begin{aligned} \Delta x(k+1) &= A\Delta x(k) + B_u \Delta u(k) \\ &\quad + B_d \Delta d(k) \\ y_c(k) &= C_c \Delta x(k) + y_c(k-1) \end{aligned} \tag{16}$$

where

$$\begin{aligned} \Delta x(k) &= x(k) - x(k-1) \\ \Delta u(k) &= u(k) - u(k-1) \\ \Delta d(k) &= d(k) - d(k-1) \end{aligned}$$

The measured value of kth at the current moment is $x(k)$, and $\Delta x(k) = x(k) - x(k-1)$ can be calculated. $\Delta x(k)$ can be used as the starting point for predicting the future dynamics of the system. From the above, the state at the $k+1$th can be predicted. This value is the state increment:

$$\Delta x(k+1|k) = A\Delta x(k) + B_u \Delta u(k) + B_d \Delta d(k) \tag{17}$$

In equation (17), "$k+1|k$" represents the prediction of the k-th time to $k+1$-th time, and the k-th time after the symbol "|" represents the current time, where the value of the $k+1$-th time does not affect the output at k-th time. After the state-space model is established, the conduction current prediction equation is derived. Then, different command values are given to the rotor converter through constraint conditions.

B. CURRENT PREDICTIVE CONTROL ALGORITHM

In the case of voltage asymmetry faults, since the stator transient flux linkage is not much and it will automatically attenuate. It also has little impact on the overvoltage. For the sake of simplicity, the influence of the stator's transient DC flux is temporarily ignored in the analysis of this paper. That is, only the positive and negative sequence flux linkage and current of the stator are considered.

Equation (9) can be rewritten as:

$$\begin{aligned} \frac{di_{r\alpha}}{dt} &= (u_{r\alpha} - e_{r\alpha} - R_r i_{r\alpha}) / \left(L_r - \frac{L_m^2}{L_s}\right) - \omega_r i_{r\beta} \\ \frac{di_{r\beta}}{dt} &= \left(u_{r\beta} - e_{r\beta} - R_r i_{r\beta}\right) / \left(L_r - \frac{L_m^2}{L_s}\right) - \omega_r i_{r\alpha} \end{aligned} \tag{18}$$

The change of the free component of the flux linkage is ignored, and the induced electromotive force $e^*_{r\alpha}$ and $e^*_{r\beta}$ are calculated. The incremental method is used to take $\Delta i_{r\alpha}$ and $\Delta i_{r\beta}$ as the output, and the forward Euler method is introduced to replace the difference quotient with the difference value. The results are the current control increment at the $k+1$th moment:

$$\begin{aligned} \Delta i_{r\alpha(k)} &= T_s \left[\frac{\Delta u_{r\alpha(k)} - \Delta e^*_{r\alpha(k)} - R_r \Delta i_{r\alpha(k)}}{L_r - L_m^2/L_s} \right. \\ &\quad \left. -\omega_r \Delta i_{r\beta(k)} \right] \\ &\quad + \Delta i_{r\alpha(k-1)} \\ \Delta i_{r\beta(k)} &= T_s \left[\frac{\Delta u_{r\beta(k)} - \Delta e^*_{r\beta(k)} - R_r \Delta i_{r\beta(k)}}{L_r - L_m^2/L_s} \right. \\ &\quad \left. -\omega_r \Delta i_{r\alpha(k)} \right] \\ &\quad + \Delta i_{r\beta(k-1)} \end{aligned} \tag{19}$$

According to the predicted future state, the output of the controlled object in the predicted time domain is calculated. And the feedback proportional coefficients f_1 and f_2 are adjusted according to the depth of the grid voltage drop. At this time, the feedback current can be written as:

$$\begin{aligned} \Delta i^*_{r\alpha}(k) &= f_1 \Delta i_{r\alpha}(k) \\ \Delta i^*_{r\beta}(k) &= f_2 \Delta i_{r\beta}(k) \end{aligned} \tag{20}$$

From the above analysis, the predicted current expression is obtained as:

$$\begin{aligned} i_{r\alpha}(k+1) &= i_{r\alpha ref}(k) + \Delta i^*_{r\alpha}(k) \\ i_{r\beta}(k+1) &= i_{r\beta ref}(k) + \Delta i^*_{r\beta}(k) \end{aligned} \tag{21}$$

Among them, the predicted value of the rotor current in equation (21) consists of two terms. They are the reference value and the incremental value. The reference value $i_{r\alpha ref}(k)$ and $i_{r\beta ref}(k)$ are the reference values obtained after the coordinate transformation of the original control strategy. The increment value $\Delta i^*_{r\alpha}(k)$ and $\Delta i^*_{r\beta}(k)$ are the results after considering the change of induced voltage and the compensation of negative sequence flux. Finally, $i_{r\alpha}(k+1)$ and $i_{r\beta}(k+1)$ will be used as the converter control signal at the k+2-th time. The improved RSC control scheme is shown in Figure 3. The green area is the traditional MPC control measurement, and the yellow area is the proposed improved MPCC strategy based on the $\alpha\beta$ coordinate system.

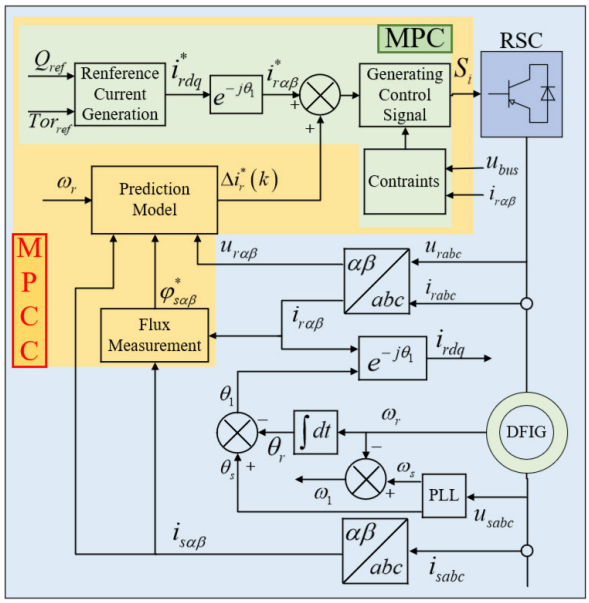

FIGURE 3. Improved rotor control strategy block diagram.

C. VALUE FUNCTION ESTABLISHMENT

Two goals of the control strategy in this paper need to be achieved. They are to achieve low voltage ride-through and ensure grid-connected power quality. These goals need to be achieved through a value function, and other goals such as reducing switching losses are not considered in this paper. Based on the above, the predicted value and the reference value of the current are obtained. Figure 4 shows the waveforms of the predicted current value and the reference current value for single-phase grounding, two-phase short-circuit, and two-phase grounding fault.

Next, the value function is created in equation (22).

$$\begin{aligned} g_a = &\left|i^*_{r\alpha}(k+1) - i_{r\alpha}(k+1)\right| \\ &+ \left|i^*_{r\beta}(k+1) - i_{r\beta}(k+1)\right| \end{aligned} \tag{22}$$

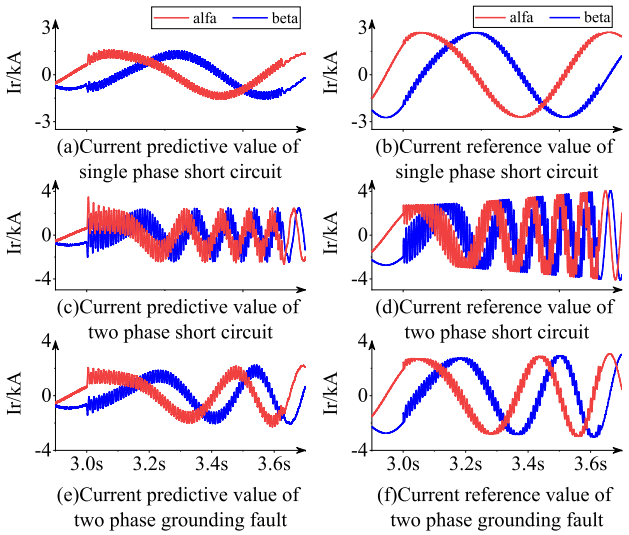

FIGURE 4. Predictive and reference values of current.

The predicted value of the current and the reference value are compared through the value function. The switch combination corresponding to the current vector that minimizes the value function is selected as the RSC trigger pulse signal, which can realize the control of the RSC. The DC bus voltage is very important for the stable operation of GSC and RSC, and the stability of the DC bus voltage is directly related to the power flowing through the bus [29]. To prevent the delay of the system from deteriorating the performance of the system, the delay is compensated according to the above-mentioned shortening the sampling time to $1/2T_s$. And it is considered to keep the DC bus voltage stable during the fault, the new value function is constructed as:

$$\begin{aligned} g_a = &\left|i^*_{r\alpha}(k+2) - i_{r\alpha}(k+2)\right| + \left|i^*_{r\beta}(k+2) - i_{r\beta}(k+2)\right| \\ &+ \lambda\left|u^*_{dc} - u_{dc}\right| \end{aligned} \tag{23}$$

The improved model predictive current control scheme is shown in Figure 5.

IV. CASE SIMULATION AND ANALYSIS

A. SIMULATION OF CLSSCB BREAKING FAULT CURRENT

To verify the proposed improved MPCC strategy, an asymmetric timing fault at the connection between the wind turbine outlet and the grid is set up in this paper. The following three working conditions of single-phase ground fault, two-phase short-circuit fault and two-phase ground fault are analyzed as examples. The improved control strategy is compared with the traditional PI control and the control scheme used in [30]. In [30], the PWM is directly output to the power converter without modulation. Later, the control strategy in [30] is expressed as traditional MPC. The grid-connected topology of the DFIG is shown in Figure 6.

Before the grid fault occurs, DFIG runs in a stable state; at 3s, an asymmetrical fault occurs on the grid with a duration

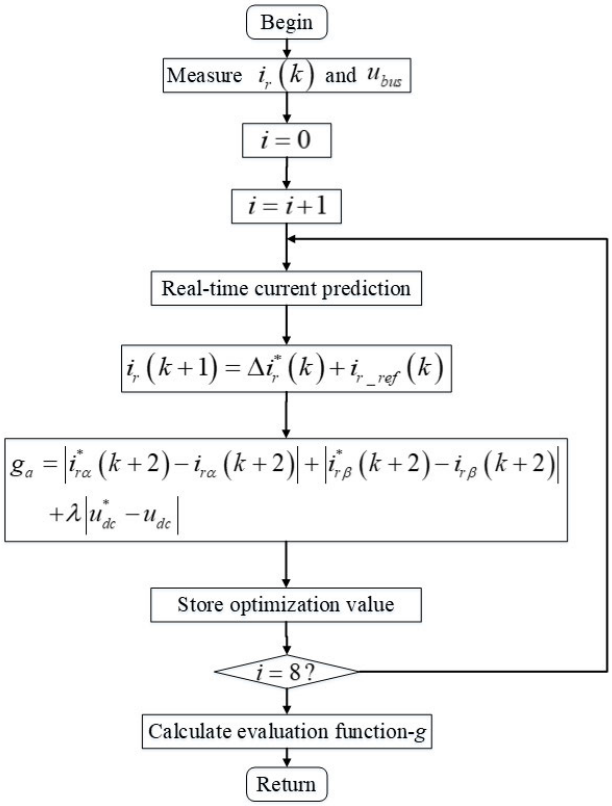

FIGURE 5. Improved model predictive current control block diagram.

of 0.625s. The main parameters of DFIG are shown in the following table:

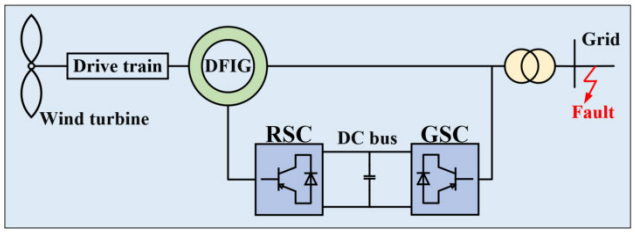

FIGURE 6. Basic structure of DFIG.

After the fault occurs, the voltage drop at the grid connection point is detected by the excitation converter. At this time, the system is switched from the original PI control to the model predictive control strategy in the paper [30] or the improved MPCC strategy. When a single-phase ground fault occurs and the grid voltage drops to 40%, the simulation waveform is shown in Figure 7; when a two-phase short-circuit fault occurs and the grid voltage drops to 50%, the simulation waveform is shown in Figure 8; when a two-phase-to-ground short-circuit fault occurs, the grid voltage drops to 50%, the simulation waveform is shown in Figure 9. From the perspective of energy flow, a sudden drop in the grid voltage will prevent all the electrical energy generated by the DFIG from being sent from the stator. The

TABLE 1. Parameter of the doubly-fed wind turbine.

Parameter	Numerical value
Stator and rotor mutual inductance (mH)	0.0025
Rotor leakage inductance (mH)	0.002587
Stator leakage inductance(mH)	0.002587
DC bus voltage reference value (kV)	1.2
Rated Capacity (MW)	2
Rated voltage (kV)	0.69
Stator resistance(mΩ)	0.0026
Rotor resistance(mΩ)	0.0029

wind energy absorbed by the wind turbine will not change significantly, which will first lead to an increase in the speed of the turbine. There is a short-term speed drop under a two-phase short circuit and two-phase grounding fault, indicating that the rotor speed is lower than its synchronous speed at this time. When the speed drops, the GSC is in the rectifying state; later, the speed gradually rises, and the GSC is in the inverter state. Figure 7-9 (a), (b), and (c) show the speed changes under different working conditions. The rising speed increases the slip energy flowing through the RSC, which leads to an increase in the rotor current. It can be seen from (d), (e), and (f) of Figure 7-9 that the quality of the rotor current waveform is stable when there is no fault. After the fault occurs, the rotor current generates a surge current due to the existence of the negative sequence component of the stator flux linkage. In the MPC scheme that does not use space vector control, the PWM control signal will be directly passed to the inverter through the minimized value function. The (e) of Figure 7-9 show that the improved control strategy has a certain inhibitory effect on the surge of current. Compared with traditional PI control and traditional MPC, the MPCC proposed in this paper makes the rotor current suppressed in the fault process better. The stator and rotor currents oscillate when the voltage drops. The degree of oscillation is not only related to speed but also related to factors such as drop depth and motor parameters. When the drop depth is too large, the overcurrent will damage the power devices of the motor.

When the terminal voltage drops, the stator voltage also drops. (j), (k) and (L) in Figure 7-9 represent the voltage drops of the b-phase stator under different working conditions. The drop of the stator voltage makes the flux chain change correspondingly, and the stator current will also have the surge current. The flux linkage is suppressed by the improved MPCC so that the stator current is suppressed. The (g), (h), and (i) of Figure 7-9 show the a-phase waveform of the stator current. It can be seen that the improved MPCC has a more obvious effect on the stator and rotor current than the traditional PI control and the traditional MPC. This is also

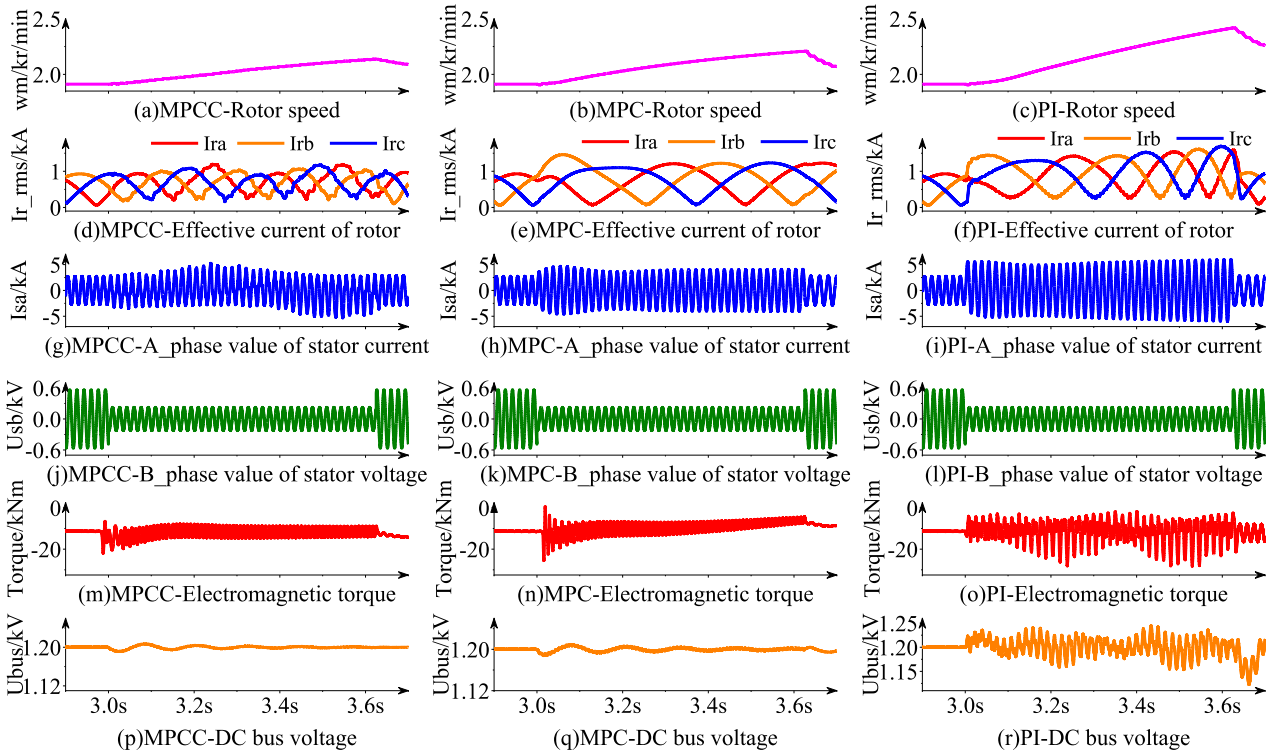

FIGURE 7. Comparison of LVRT performance between improved MPCC and traditional MPC and PI for single-phase grounding.

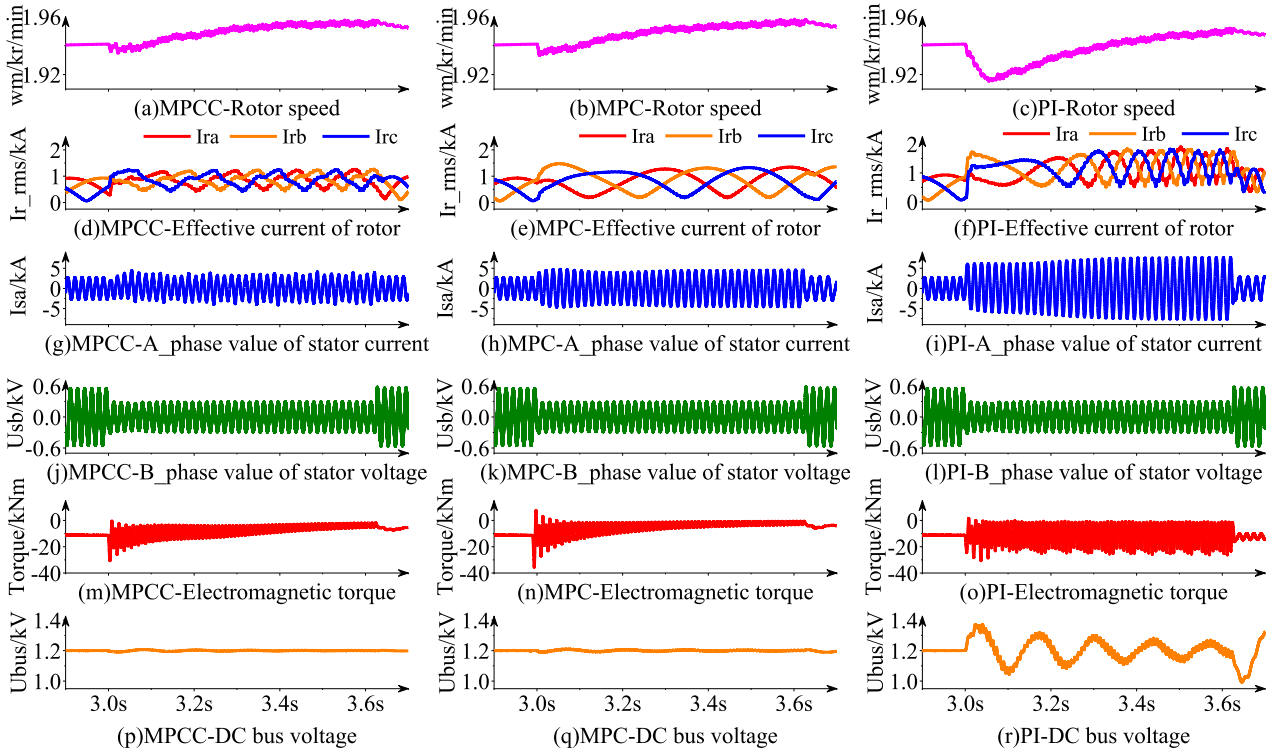

FIGURE 8. Comparison of LVRT performance between improved MPCC and traditional MPC and PI in two-phase short circuit.

conducive to controlling the stator to send reactive power through the rotor current after the voltage drops, to provide reactive power support to the grid.

To suppress the over-voltage and over-current phenomenon on the rotor side when the grid voltage drops, it is necessary to suppress the induced electromotive force on the rotor side.

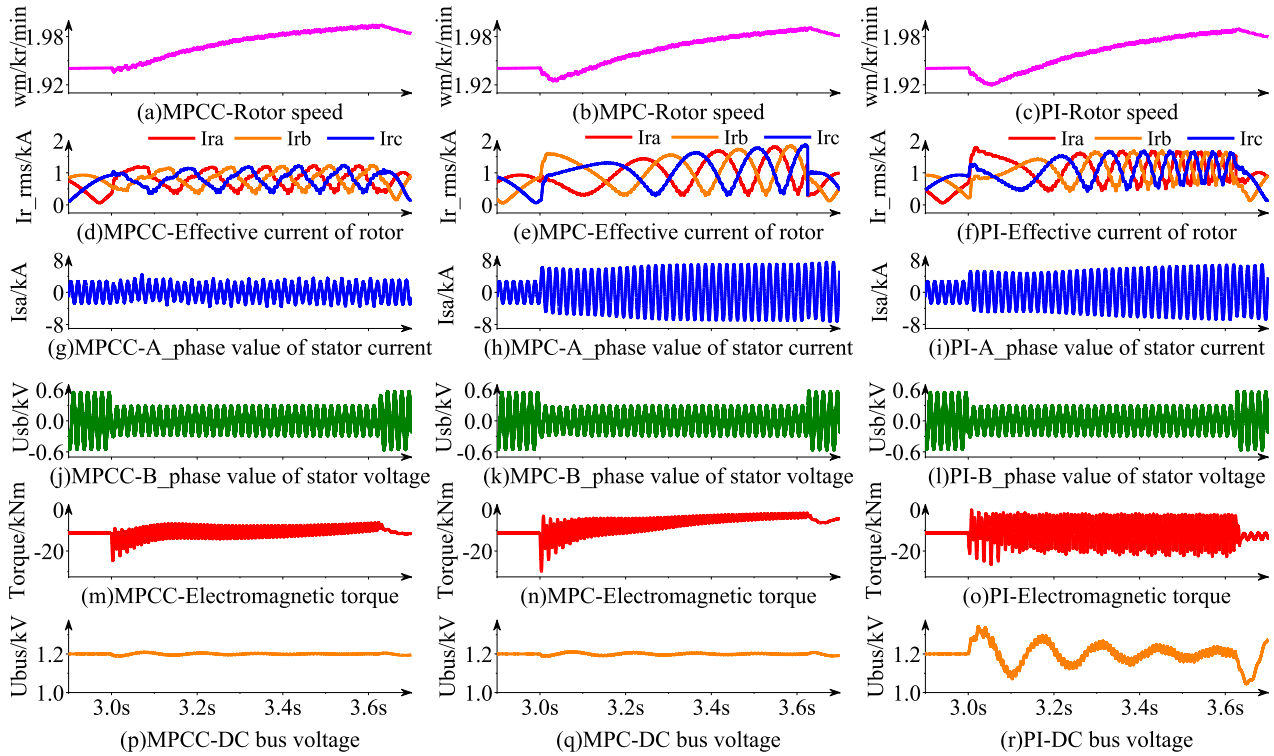

FIGURE 9. Comparison of LVRT performance between improved MPCC and traditional MPC and PI in two-phase short grounding.

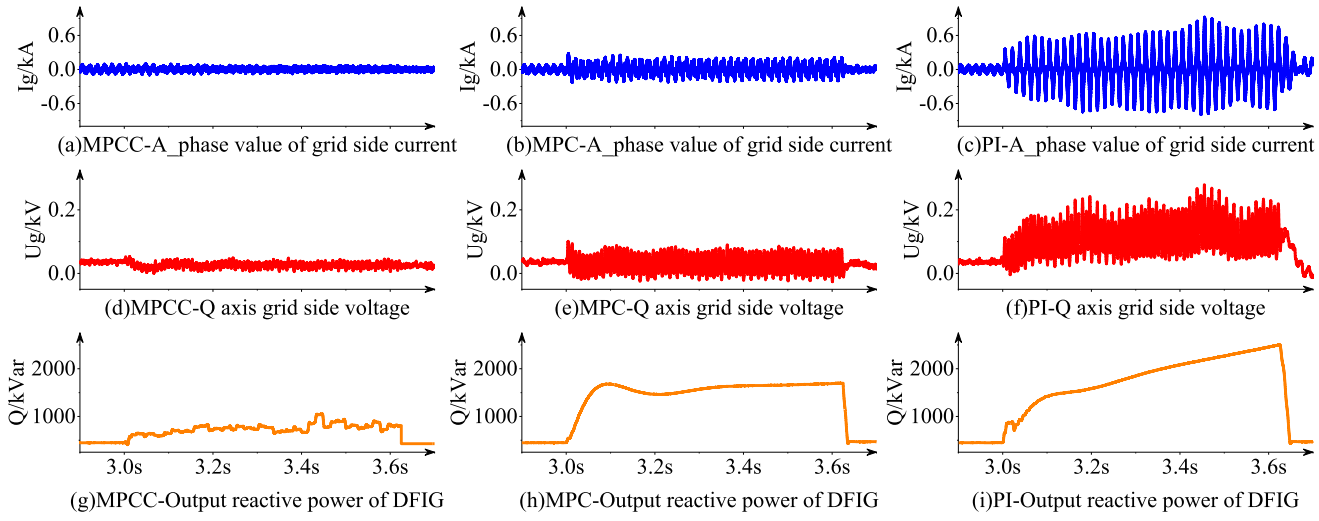

FIGURE 10. Comparison of LVRT performance between improved MPCC and traditional MPC and PI for single-phase grounding.

This induced electromotive force is generated by the AC component of the stator flux and the DC component of the rotating and cutting rotor windings. In the above analysis, the DC component and its influence have been ignored. Therefore, the essence of fault control is to suppress the AC component of the flux linkage caused by the fault. It can be seen from Figure 7-9, where (o) indicates that the electromagnetic torque under the traditional PI control has a large number of double-frequency AC components generated by the flux cutting. PI control cannot be effectively suppressed due to its control limitations. The traditional MPC represented in (n) has a certain inhibitory effect on the electromagnetic torque. Although the amplitude is large, it will also have a restraining effect over time. But because it does not suppress

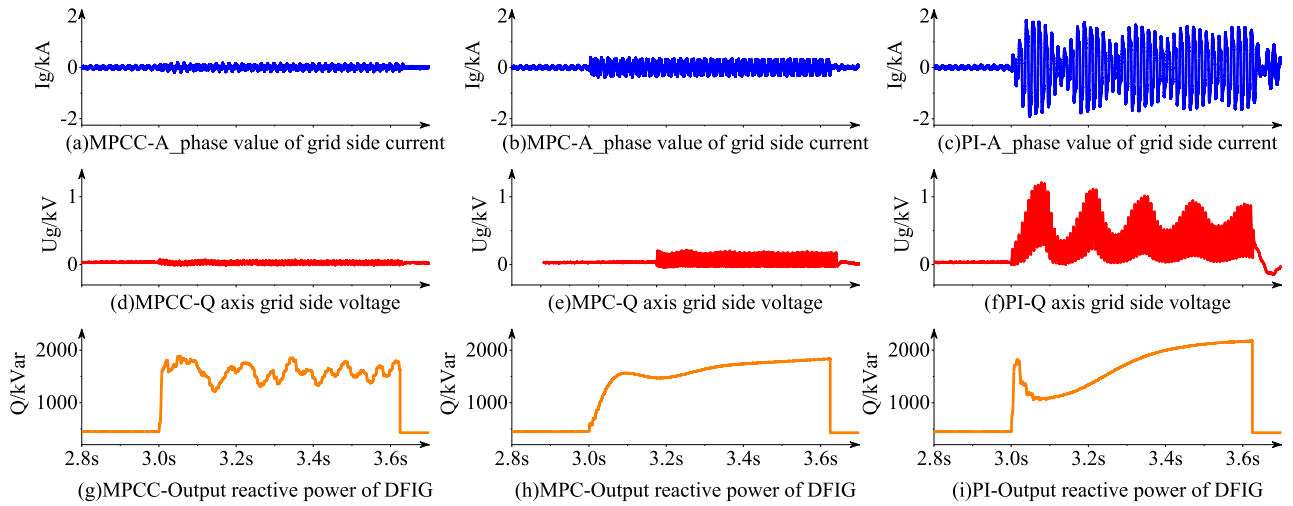

FIGURE 11. Comparison of LVRT performance between improved MPCC and traditional MPC and PI in two-phase short circuit.

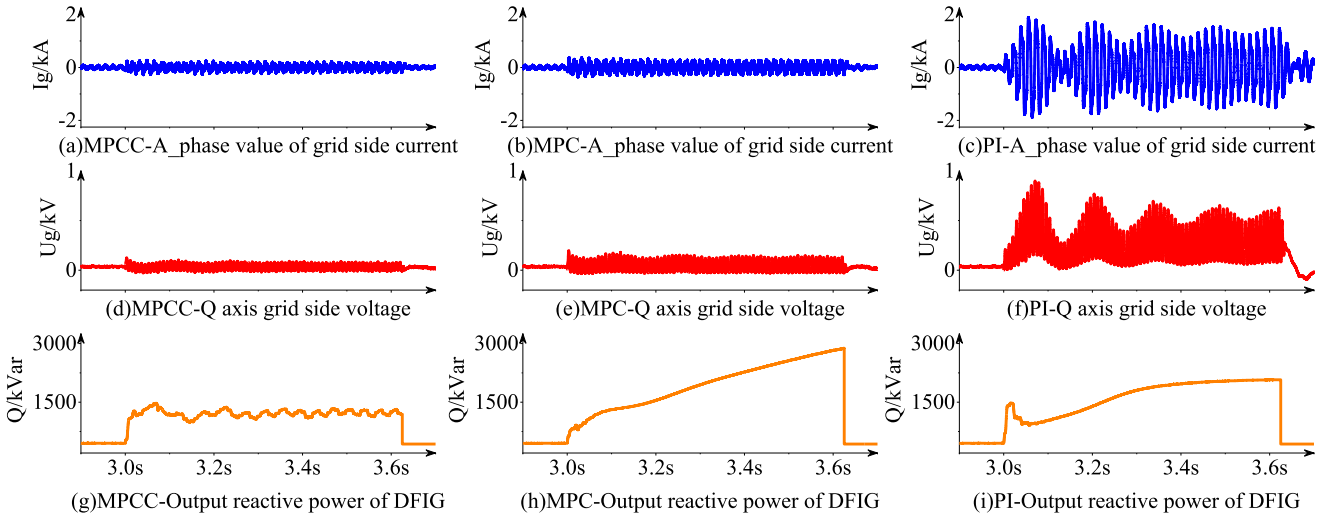

FIGURE 12. Comparison of LVRT performance between improved MPCC and traditional MPC and PI in two-phase short grounding.

the double frequency AC component, the control is not stable enough. The improved MPCC shown in (m) means that the double-frequency AC component is suppressed so that the electromagnetic torque decays quickly and the oscillation amplitude is small. At this time, the fluctuation is unavoidable but relatively stable.

No matter what control strategy is adopted by the RSC and the GSC during the fault period, it is required to ensure the stability of the DC bus voltage. To ensure the stability of the DC bus voltage is to ensure the controllability of the GSC. This is a prerequisite for the normal operation of the excitation converter and the effectiveness of the improved control strategy. Figure 7-9 (p), (q), and (r) correspond to the DC bus voltage changes of the converter based on PI control, traditional MPC, and improved MPCC, respectively. It can be seen from the waveform before 3s that the DC bus voltage is stable at about 1.2kV when there is no fault. When a fault occurs, energy will be accumulated at the DC bus, and the DC bus voltage will oscillate. Moreover, the voltage oscillation under a two-phase fault is more serious than a single-phase ground fault. The fluctuations can be suppressed by the improved MPCC strategy and the suppression rate over time during the fault period is accelerated. In the improved MPCC, the DC bus voltage is taken into consideration to make the suppression effect better, and the harmonic content is reduced. It can be seen that no matter for single-phase grounding, two-phase short circuit, or two-phase short grounding, the improved MPCC strategy proposed in this paper is better

than the traditional PI controller and the traditional MPC in ensuring the stability of the DC bus voltage. In addition, the suppression effect of two-phase short circuit and two-phase short grounding is more obvious than that under single-phase grounding. At 3.625s, the grid voltage is restored, and the magnetic field will suddenly change again to make the current oscillate. Since the MPCC has a certain inhibitory effect on the electromagnetic torque, the electromagnetic torque is in a relatively stable state when switching to PI control, so the fluctuation is not large. Therefore, the DC bus voltage is not affected too much. But its fluctuation cannot be effectively suppressed under the control of traditional PI for a long time.

Figure 10-12 are the grid-side current, voltage, and output reactive power waveforms in the d-q coordinate system. They are the waveforms of improved MPCC, traditional MPC, and traditional PI control when the single-phase fault voltage drops to 40%, the voltage drops to 50% under a two-phase short circuit, and the voltage drops to 50% under a two-phase short grounding. In the case of a grid failure, the quality of the grid-connected voltage and current waveforms can be improved by the improved MPCC strategy. The q-axis reference value u^*_{qgref} of the GSC is based on the DC bus voltage as the control target. Figure 10-12 (d), (e), and (f) show that both the traditional MPC and the improved MPCC control can suppress the u_{qg} oscillation, which is consistent with the above analysis of DC bus voltage. The above analysis shows that the improved MPCC effectively guarantees the stability of the DC bus voltage. At this time, the GSC is in a controllable state and the control effect is better than the traditional MPC. Therefore, the suppression effect on the grid-side voltage and current waveforms is more obvious than that of the traditional MPC.

Figure 10-12 (g), (h), and (i) are reactive power waveforms. It can be seen from the figure that when the voltage drops, DFIG will inject a certain amount of reactive power into the grid, and the measured reactive power will increase at this time. The fault is cleared at 3.625s, after a short-term transient, the reactive power will directly recover to the steady-state value before the fault occurs. The analysis shows that the stator overcurrent and the rotor overcurrent are effectively restrained by the improved MPCC so that the reactive power of the stator is in a controllable state under single-phase grounding. Although the traditional MPC has a certain inhibitory effect, it cannot effectively track the reactive power.

V. CONCLUSION

The transient characteristics of DFIG under asymmetric faults are analyzed in this paper and an improved MPCC method without adding hardware protection equipment is proposed. Based on the above analysis, the following conclusions are obtained:

1) An improved MPCC strategy based on asymmetrical faults in the power grid under the $\alpha\beta$ coordinate system is proposed in this paper. Different from traditional PI and traditional MPC, the calculation amount of the improved MPCC strategy is greatly reduced. And in this strategy, the positive and negative sequence separation of the current is not needed. A new measurement structure of flux linkage was proposed, which simplifies the links of flux linkage. The model sampling time is set to offset the minimum step length of the predictive control delay, which effectively solves the problem of one-beat delay in MPCC.
2) The simulation verification is carried out for the single-phase grounding, the two-phase short circuit, and the two-phase short grounding. The results show that the two control objectives of LVRT, namely, self-protection and support, are achieved by the improved MPCC strategy.

REFERENCES

[1] H. T. Jadhav and R. Roy, "A comprehensive review on the grid integration of doubly fed induction generator," *Int. J. Elect. Power Energy Syst.*, vol. 49, pp. 8–18, Jul. 2013.

[2] Y. E. Karkri, A. B. Rey-Boué, H. E. Moussaoui, J. Stöckl, and T. I. Strasser, "Improved control of grid-connected DFIG-based wind turbine using proportional-resonant regulators during unbalanced grid," *Energies*, vol. 12, no. 21, p. 4041, Oct. 2019.

[3] W. Li, P. Chao, X. Liang, Y. Sun, J. Qi, and X. Chang, "Modeling of complete fault ride-through processes for DFIG-based wind turbines," *Renew. Energy*, vol. 118, pp. 1001–1014, Apr. 2018.

[4] M. M. Moghimian, M. Radmehr, and M. Firouzi, "Series resonance fault current limiter (SRFCL) with MOV for LVRT enhancement in DFIG-based wind farms," *Electric Power Compon. Syst.*, vol. 47, nos. 19–20, pp. 1814–1825, Dec. 2019.

[5] T. L. Van, T. H. Nguyen, N. M. Ho, X. N. Doan, and T. H. Nguyen, "Voltage compensation scheme for DFIG wind turbine system to enhance low-voltage ride-through capability," in *Proc. 10th Int. Conf. Power Electron. ECCE Asia (ICPE-ECCE Asia)*, May 2019, pp. 1334–1338.

[6] A. M. Rauf, V. Khadkikar, and M. S. El Moursi, "A new fault ride-through (FRT) topology for induction generator based wind energy conversion systems," *IEEE Trans. Power Del.*, vol. 34, no. 3, pp. 1129–1137, Jun. 2019.

[7] P. Piya, M. Ebrahimi, M. K. Ghartemani, and S. A. Khajehoddin, "Fault ride-through capability of voltage-controlled inverters," *IEEE Trans. Ind. Electron.*, vol. 65, no. 10, pp. 7933–7943, Feb. 2019.

[8] X. Liu, Z. Xu, and K. P. Wong, "Recent advancement on technical requirements for grid integration of wind power," *J. Modern Power Syst. Clean Energy*, vol. 1, no. 3, pp. 216–222, Dec. 2013.

[9] H. Guo, D. Z. Huang, L. G. Gu, and F. Y. Wu, "Model of DFIG wind farm and study on its LVRT capability," *J. Electron. Sci. Technol.*, vol. 11, no. 1, pp. 78–83, Mar. 2013.

[10] S. Li, S. Qin, R. Wang, Q. Li, and C. Chen, "Study on grid adaptability testing methodology for wind turbines," *J. Modern Power Syst. Clean Energy*, vol. 1, no. 1, pp. 81–87, Jul. 2013.

[11] M. Tsili and S. Papathanassiou, "A review of grid code technical requirements for wind farms," *IET Renew. Power Generat.*, vol. 3, no. 3, pp. 308–332, Sep. 2009.

[12] D. Campos-Gaona, E. L. Moreno-Goytia, and O. Anaya-Lara, "Fault ride-through improvement of DFIG-WT by integrating a two-degrees-of-freedom internal model control," *IEEE Trans. Ind. Electron.*, vol. 60, no. 3, pp. 1133–1145, Mar. 2013.

[13] M. Mohseni, S. Islam, and M. A. S. Masoum, "Fault ride-through capability enhancement of doubly-fed induction wind generators," *IET Renew. Power Gener.*, vol. 5, no. 5, pp. 368–376, Sep. 2011.

[14] M. Mohseni and S. M. Islam, "Transient control of DFIG-based wind power plants in compliance with the Australian grid code," *IEEE Trans. Power Electron.*, vol. 27, no. 6, pp. 2813–2824, Jun. 2012.

[15] I. Villanueva, A. Rosales, P. Ponce, and A. Molina, "Grid-voltage-oriented sliding mode control for DFIG under balanced and unbalanced grid faults," *IEEE Trans. Sustain. Energy*, vol. 9, no. 3, pp. 1090–1098, Jul. 2018.

[16] Z. Dao and F. Blaabjerg, "Optimized demagnetizing control of DFIG power converter for reduced thermal stress during symmetrical grid fault," *IEEE Trans. Power Electron.*, vol. 33, no. 12, pp. 10326–10340, Dec. 2018.

[17] Y.-W. Shen, D.-P. Ke, W. Qiao, Y.-Z. Sun, D. S. Kirschen, and C. Wei, "Transient reconfiguration and coordinated control for power converters to enhance the LVRT of a DFIG wind turbine with an energy storage device," *IEEE Trans. Energy Convers.*, vol. 30, no. 4, pp. 1679–1690, Dec. 2015.
[18] X. Liao, H. Li, R. Yao, Z. Huang, and K. Wang, "Voltage overshoot suppression for SiC MOSFET-based DC solid-state circuit breaker," *IEEE Trans. Compon., Packag., Manuf. Technol.*, vol. 9, no. 4, pp. 649–660, Apr. 2019.
[19] M. Morari and J. H. Lee, "Model predictive control: Past, present and future," *Comput. Chem. Eng.*, vol. 23, nos. 4–5, pp. 667–692, May 1999.
[20] S. Kouro, P. Cortes, R. Vargas, U. Ammann, and J. Rodriguez, "Model predictive control—A simple and powerful method to control power converters," *IEEE Trans. Power Electron.*, vol. 56, no. 6, pp. 1826–1838, Jun. 2009.
[21] M. E. Zarei, C. V. Nicolás, and J. Rodríguez Arribas, "Improved predictive direct power control of doubly fed induction generator during unbalanced grid voltage based on four vectors," *IEEE J. Trans. Emerg. Sel. Topics Power Electron.*, vol. 5, no. 2, pp. 695–707, Jun. 2017.
[22] J. Hu, J. Zhu, and D. G. Dorrell, "Predictive direct power control of doubly fed induction generators under unbalanced grid voltage conditions for power quality improvement," *IEEE Trans. Sustain. Energy*, vol. 6, no. 3, pp. 943–950, Jul. 2015.
[23] M. K. Döşoğlu, "A new approach for low voltage ride through capability in DFIG based wind farm," *Int. J. Elect. Power Energy Syst.*, vol. 83, pp. 251–258, Dec. 2016.
[24] J. Luo, *Optimization Strategy of Doubly-Fed Fan During Low Voltage Crossing Based on Model Predictive Control*. Jinan, China: Shandong Univ., 2020.
[25] Z. Li, J. F. An, Y. Xiao, Q. S. Zhang, and H. X. Sun, "Design of model predictive control system for permanent magnet synchronous linear motor based on adaptive observer," *Trans. China Electrotech. Soc.*, vol. 36, no. 6, pp. 1190–1200, Mar. 2021.
[26] S. Zeng, Z. Chen, X. Tan, J. X. He, and P. Tian, "Grid-connected strategy of doubly-fed machines based on model prediction," *Sci. Technol. Eng.*, vol. 19, no. 23, pp. 113–119, Aug. 2019.
[27] B. F. Zhang, J. M. Xu, and S. J. Xie, "Analysis and suppression of the aliasing in real-time sampling for grid-connected LCL-filtered inverters," *Proc. CSEE*, vol. 36, no. 15, pp. 4192–4203, Aug. 2016.
[28] X. L. Yao, C. Q. Huang, J. F. Wang, M. He, and T. Z. Liu, "Model predictive power control of permanent magnet synchronous motor in two-phase static coordinate system," *Trans. China Electrotech. Soc.*, vol. 36, no. 1, pp. 60–67, Jan. 2021.
[29] H. Y. Dong, Z. J. Tang, R. P. Zhang, and P. L. Yang, "Zero-voltage crossing control method for photovoltaic inverter based on model predictive modulation function under asymmetric faults," *Acta Energiae Solaris Sinica*, vol. 40, no. 6, pp. 1616–1625, Jun. 2019.
[30] J. R. Rodriguez, M. P. Kazmierkowski, J. R. Espinoza, P. Zanchetta, H. Abu-Rub, H. A. Young, and C. A. Rojas, "State of the art of finite control set model predictive control in power electronics," *IEEE Trans. Ind. Informat.*, vol. 9, no. 2, pp. 1003–1016, May 2013.

CAN DING was born in Shandong, China. He received the B.S. and M.S. degrees in electrical engineering from Xi'an Jiao Tong University (XJTU), Xi'an, China, in 2005 and 2010, respectively, and the Ph.D. degree in electrical engineering from the Huazhong University of Science and Technology (HUST), Wuhan, China, in 2018.

He has been a Lecturer with the College of Electrical Engineering & New Energy, China Three Gorges University (CTGU). His current research interests include high voltage electrical design and the application of artificial intelligence in images.

YUNWEN CHEN received the B.S. degree from the North China University of Water Resources and Electric Power (NCWU), Zhengzhou, China, in 2019. She is currently pursuing the M.S. degree in electrical engineering with China Three Gorges University (CTGU). Her research interests include wind power grid and DC micro-networks.

TAIPING NIE received the B.S. degree from Hubei Normal University (HNU), Huangshi, China, in 2019. He is currently pursuing the M.S. degree in electrical engineering with China Three Gorges University (CTGU). His research interests include topology design of DC circuit breakers and high-voltage insulation techniques.